ACS APPLIED MATERIALS & INTERFACES

Research Article

www.acsami.org

Colloidal PbSe Solar Cells with Molybdenum Oxide Modified Graphene Anodes

Hua Wu,[†,§] Xiaoyu Zhang,[†] Yu Zhang,[*,†,‡] Long Yan,[†] Wenzhu Gao,[‡] Tieqiang Zhang,[‡] Yiding Wang,[†] Jun Zhao,[∥] and William W. Yu[*,†,§,∥]

[†]State Key Laboratory on Integrated Optoelectronics and College of Electronic Science and Engineering and [‡]State Key Laboratory of Superhard Materials and College of Physics, Jilin University, Changchun 130012, China

[§]College of Material Science and Engineering, Qingdao University of Science and Technology, Qingdao 266042, China

[∥]Department of Chemistry and Physics, Louisiana State University, Shreveport, Louisiana 71115, United States

ABSTRACT: With good electrical conductivity, optical transparency, and mechanical compliance, graphene films have shown great potential in application for photovoltaic devices as electrodes. However, photovoltaic devices employing graphene anodes usually suffer from poor hole collection efficiency because of the mismatch of energy levels between the anode and light-harvesting layers. Here, a simple solution treatment and a low-cost solution-processed molybdenum oxide (MoO_x) film were used to modify the work function of graphene and the interfacial morphology, respectively, yielding highly efficient hole transfer. As a result, the graphene/MoO_x anodes demonstrated low surface roughness and high electrical conductivity. Using the graphene/MoO_x anodes in PbSe nanocrystal solar cells, we achieved 1 sun power conversion efficiency of 3.56%. Compared to the control devices with indium tin oxide anodes, the graphene/MoO_x-based devices show excellent performance, demonstrating the great potential of the graphene/MoO_x anodes for use in optoelectronics.

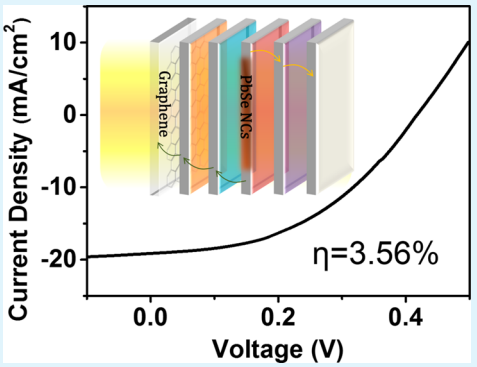

KEYWORDS: *graphene, solution-processed MoO_x, PbSe nanocrystal, solar cell, hole transfer*

1. INTRODUCTION

Indium tin oxide (ITO) has been widely used as a transparent conducting electrode material in optoelectronics devices. However, the rising cost and brittleness of ITO limit the use of this oxide material.[1] Meanwhile, the surface roughness (root-mean-square, rms) of the ITO film is high (~4.8 nm) because of its polycrystalline nature,[2] and an ITO-based electrode has instable work function under different processing conditions.[3] Therefore, there is a crucial demand to develop other novel electrode materials with good stability, high transparency, and excellent conductivity for optoelectronic application.

Graphene is a single atomic layer of carbon hexagons. It has attracted much attention as electrode material because of its numerous advantages including low cost, high transparency, high planar electrical conductivity, chemical robustness, and flexibility.[4−8] However, the low work function of graphene film may limit the performance of solar cells with graphene electrodes. To solve the problem, several methods have been proposed, such as chemical doping,[9−13] polymer material modification,[14] and transition metal oxide modification.[15−17] Among the above-mentioned methods, metal oxide modification with MoO_3, NiO_x, or TiO_2 was most widely employed. Previous studies have shown that the introduction of a MoO_3 layer can increase the anode work function and improve the film surface morphology, which will enhance the hole collection efficiency and produce a low ohmic contact resistance.[16] However, it is costly and time-consuming to deposit these metal oxides via vacuum deposition technique. Therefore, there is an urgent demand for the development of low-cost solution-processed anode modification material.

Photovoltaics based on semiconductor nanocrystals (NCs) have attracted much attention because of their facile solution processing, quantum-size-effect band gap tunability, and multiexciton generation effect.[18−28] Since the report of the first NCs solar cell in 2005,[29] there have been steady improvements in the power conversion efficiency of NC-based photovoltaics, enabled by both new device architectures[30,31] and improved NC films.[32,33] Encouraging efficiencies have been achieved exceeding 8.5%.[34,35] However, the study of NC solar cells based on graphene electrodes has been rarely reported.[36,37] In this work, graphene anode modified by solution-processed molybdenum oxide was introduced and employed in a PbSe NC solar cell device. Compared to the control samples based on ITO anodes, the graphene-based devices have shown good performance, indicating the great potential of monolayer graphene films for application in optoelectronics.

Received: May 5, 2015
Accepted: September 10, 2015
Published: September 10, 2015

DOI: 10.1021/acsami.5b03894
ACS Appl. Mater. Interfaces 2015, 7, 21082−21088

2. EXPERIMENTAL SECTION

2.1. Graphene Growth, Transfer, and Chemical Doping. Monolayer graphene was produced via a chemical vapor deposition (CVD) process, following the methods reported previously.[15,38−42] Using a piece of Cu foil as a substrate for growth, a monolayer graphene film over the whole area of the wafer was obtained. After that, the graphene film was transferred to quartz substrate by a poly(methyl methacrylate) (PMMA)-assisted transfer technique. To improve the sheet resistance of the graphene film, the graphene samples were soaked into 1 mg/mL triethyloxonium hexachloroantimonate/dichloroethene solution for 30 min.[43]

2.2. PbSe NCs Synthesis. PbSe NCs were synthesized by modifying a literature method.[44−46] The synthesis was carried out in a three-necked flask with condenser, magnetic stirrer, thermocouple, and heating mantle. The reaction mixture containing lead(II) oxide (Aladdin, 99.99%, 0.892 g), oleic acid (Alfa Aesar, 90%, 5 mL), and 1-octadecene (ODE) (Alfa Aesar, 90%, 12 mL) turned colorless upon heating to 180 °C under nitrogen. Subsequently, 8 mL of 1.0 M Se-tributylphosphine (containing 0.64 g Se) was rapidly injected into the reaction flask under nitrogen when the temperature of reaction system was adjusted to 90 °C. The monodisperse PbSe NCs were achieved after growing for 3 min at 75 °C. The reaction was quenched by the injection of 50 mL of methanol. The purification was carried out following the approach that has been well-established.[47−49] The obtained PbSe NCs were dissolved in octane and stored in a nitrogen-filled glovebox for device fabrication.

2.3. ZnO NCs Synthesis. ZnO NCs were synthesized via a previously reported method.[50] A mixture of zinc acetate dihydrate (Acros, > 98%, 2.95 g) and methanol (125 mL) was loaded into a three-necked flask and heated to 60 °C. A solution of potassium hydroxide (Merck, 87%, 1.48 g) in methanol (65 mL) was slowly added to the flask, and the solution was kept stirring for 2.5 h. ZnO NCs were washed twice by methanol and redispersed in chloroform.

2.4. Device Fabrication. The layer of MoO_x film was deposited on top of the graphene surface by spin-coating (4000 rpm) $MoO_2(acac)_2$ isopropanol (5 mg/mL) solution, annealed in air at 150 °C for 10 min to form MoO_x, and then treated under UV−ozone for 15 min.[2,51,52] Then, a layer of poly(ethylenedioxythiophene):polystyrenesulfonate (PEDOT:PSS) (~40 nm thickness) was spin-coated on the surface of MoO_x-modified graphene (or precleaned ITO-coated glass) and annealed for 10 min at 150 °C in air. PbSe NC film (~220 nm thickness) was fabricated via layer-by-layer spin-coating using a solution of PbSe NCs dispersed in octane (60 mg/mL). For each layer, after spin-coating PbSe solution onto the substrate, a 0.001 M 1,3-benzenedithiol (BDT) solution in acetonitrile was applied to the substrate, followed by rinse/spin steps with toluene to remove excess BDT and ligands. ZnO NCs film was fabricated by spin-coating a solution of ZnO NCs onto the BDT-treated PbSe NC film and drying at 90 °C for 30 min in the glovebox. Al cathode (100 nm thickness) was deposited by thermal evaporation at a pressure of ~1×10^{-6} Torr. The active area of device was 4 mm^2 as defined by the overlap of the anode and cathode.

2.5. Characterizations. Absorption spectra and optical transmittance were recorded via a PerkinElmer Lambda 950 UV−vis spectrophotometer. Photoluminescence (PL) spectra were recorded on a PerkinElmer LS50B spectrophotometer. TEM studies were carried out using a TECNAI F30ST TEM operated at 300 kV. A 4 μL NC solution was placed on an ultrathin carbon-film-coated copper grid until dry. The surface morphologies of graphene, MoO_x, and PEDOT:PSS films were analyzed using a VEECO DICP-II atomic force microscope (AFM) under ambient conditions at room temperature. Current density−voltage characteristic of the solar cell devices were measured using a Keithley 2612B sourcemeter under simulated 1 sun illumination. The illumination-integrated intensity was set to 100 mW/cm^2 using a calibrated single-crystalline silicon reference cell.

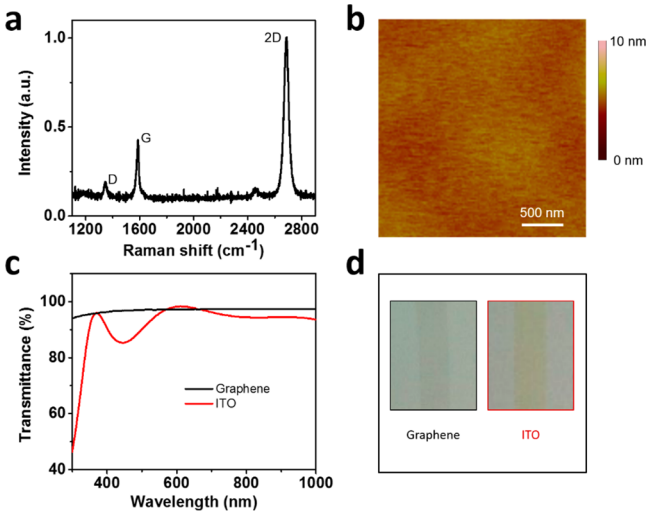

Figure 1. (a) Raman spectrum of the monolayer graphene film on quartz substrate. (b) AFM image of the single layer graphene film. (c) Transmission spectra of graphene on quartz and ITO on glass. (d) Pictures of graphene film on quartz substrate and ITO film on glass substrate (center columns).

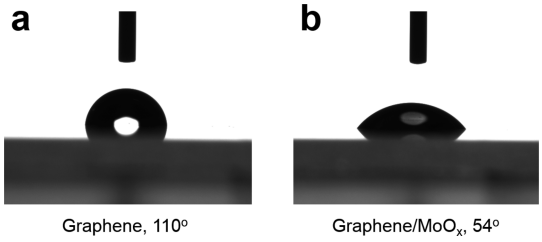

Figure 2. Static contact angles of (a) graphene anode and (b) MoO_x-modified graphene.

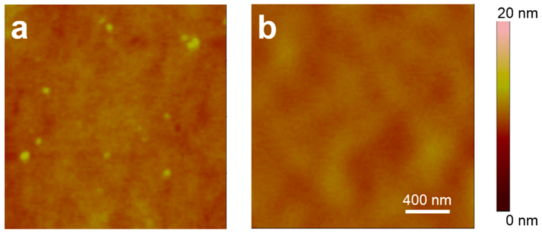

Figure 3. AFM images of the surface of (a) MoO_x on graphene film and (b) PEDOT:PSS on graphene/MoO_x anode.

3. RESULTS AND DISCUSSION

Figure 1a shows the Raman spectrum of the graphene film on quartz substrate, which has two peaks around 1587 cm^{-1} (G peak) and 2686 cm^{-1} (2D peak). The ratio of G/2D intensity (I_G/I_{2D}) was about 0.42, indicating that the graphene film was monolayer. Furthermore, it can be observed that the defect-related D band around 1345 cm^{-1} is small, indicating the low disorder and high quality of the graphene film.[53]

The transparency and surface morphology of the anode are important for good device performance, so we carried out AFM and optical transmittance characterizations of the monolayer graphene film. Figure 1b shows that the surface roughness (rms) of graphene film is 0.3 nm, suggesting a smooth surface of graphene film, whereas Figure 1c shows the measured transmittance of the graphene film and ITO. The transmittance of graphene film was around 97% across the visible spectral

DOI: 10.1021/acsami.5b03894
ACS Appl. Mater. Interfaces 2015, 7, 21082−21088

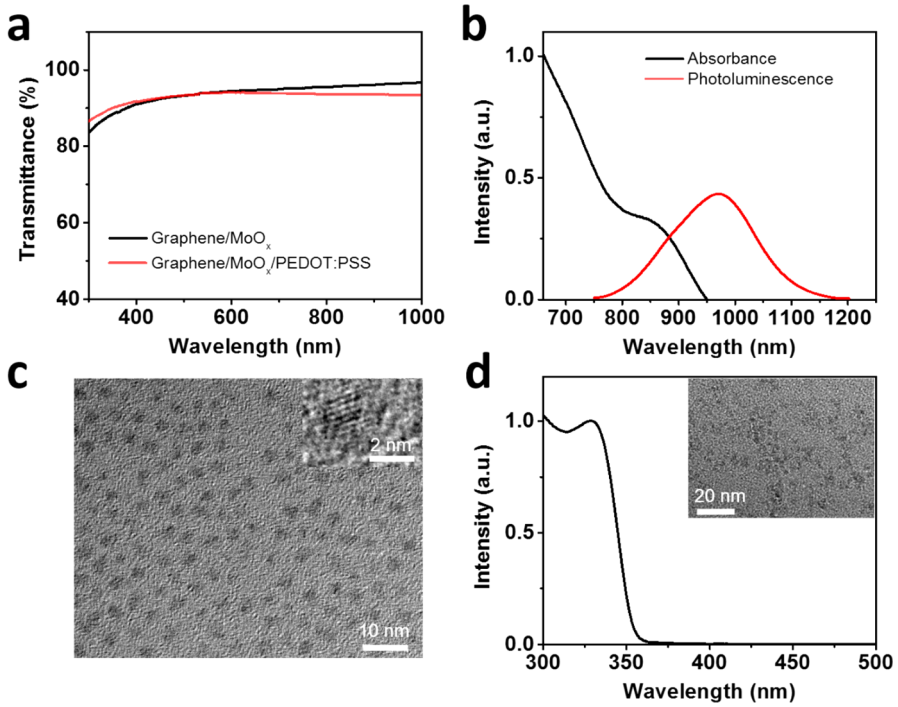

Figure 4. (a) Optical transmittance of MoO_x and MoO_x/PEDOT:PSS on graphene substrate. (b) Absorption and photoluminescence spectra of PbSe NCs in octane. (c) TEM image of the PbSe NCs. Inset: typical PbSe nanoparticle. (d) Absorption spectra of ZnO film and the TEM image of the ZnO NCs.

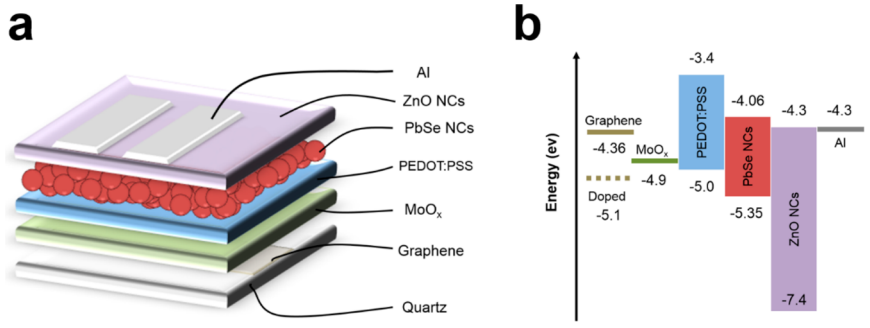

Figure 5. (a) Device structure and (b) corresponding energy level diagram of the fabricated photovoltaic device. The energy levels of materials are based on the literature.[16,52,58,59]

range, whereas ITO film had a transmittance peaks at 612 nm. It can be concluded that graphene film has higher transmittance than ITO film, which can be observed visually from the photos of graphene film on quartz substrate and ITO film on glass substrate (Figure 1d). The π-conjugated system in graphene results in light absorption, which means that the transparency of the graphene film will be higher as the graphene film becomes thinner. However, an increase in the sheet resistance of the graphene films will be observed. The single-layer graphene film was found to have a typical sheet resistance of 1.1 kΩ/sq at room temperature, which decreased to 400 Ω/sq after doping by triethyloxonium hexachloroantimonate.

Although such monolayer graphene film has clearly exhibited its high quality, it is important to apply this material into working NC solar cells in order to evaluate its performance as an electrode material. The surface free energy and work function of the electrodes have great influence on device performance. In a conventional PbSe NC-based solar cell, PEDOT:PSS is spin-coated on ITO anode to block electron transport and to aid in hole collection. The active layer of PbSe NCs is sandwiched between an ITO/PEDOT:PSS anode and a low-work-function cathode. However, in the case of graphene anode, prior to the deposition of PEDOT:PSS layer, an additional interfacial modification layer (MoO_x) is required to cover the graphene film. This process is critical in graphene-based NC solar cells because of the poor hydrophility and low work function of the graphene anode. Figure 2a shows the static contact angles of graphene anode and solution-processed MoO_x-modified graphene. The pristine graphene substrate had a contact angle of 110°, whereas the MoO_x-modified graphene anode had a contact angle of 54°, indicating the improvement of hydrophilicity induced by the addition of the MoO_x layer.

Because the surface smoothness and transparency of electrode materials are important for good device performance, we investigated the performance of the graphene/MoO_x anode via several routes. First, the surface morphology of graphene/MoO_x anode was characterized using AFM. Figure 3a shows that the surface of MoO_x film spin-coated on graphene anode is smooth, with a rms of 0.50 nm. Figure 3b shows the surface of PEDOT: PSS layer deposited on MoO_x/graphene, with a rms

DOI: 10.1021/acsami.5b03894
ACS Appl. Mater. Interfaces 2015, 7, 21082−21088

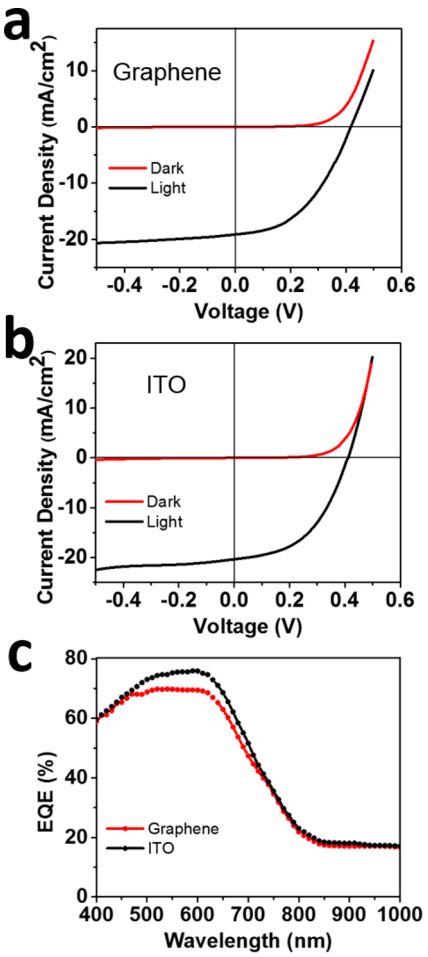

Figure 6. $J-V$ characteristics of solar cell devices fabricated on (a) graphene/MoO_x and (b) ITO under dark (red) and 100 mW/cm^2 AM1.5G spectral illumination (black). (c) EQEs of of PbSe solar cells fabricated on the graphene and ITO anodes.

of 0.39 nm, indicating that PEDOT:PSS can wet the surface of the graphene anode efficiently after being modified by MoO_x. The smooth films result in low ohmic contact resistance and stable electrical conduction across the device.

In addition, we investigated the transmittance of MoO_x-modified graphene anode, as shown in Figure 4a. The graphene/MoO_x anode was relatively transparent with transmittance ranging from 90–96% across the visible spectral range, which is favorable for light harvesting. Furthermore, the anode was still highly transparent after being deposited with a PEDOT:PSS layer.

In view of the smooth film surface and high transparency of the graphene anode modified by MoO_x, we employed the graphene/MoO_x anode into a working solar cell, with a PEDOT: PSS layer as the hole transport layer (HTL), PbSe NCs (2.6 nm) as the active layer, and a ZnO layer as the electron transport layer (ETL). The absorption and PL spectra of PbSe NCs are shown in Figure 4b. The absorption curve showed a peak at 870 nm, whereas the PL spectrum peaked at 984 nm. Figure 4c shows the TEM image of PbSe NCs, exhibiting an average diameter of 2.6 nm. A typical PbSe nanoparticle is shown in the inset of Figure 4c, indicating good crystallinity of the NCs without detectable stacking faults or crystal defects. Figure 4d shows the absorption spectrum of ZnO NCs around 4.9 nm, with an inset of a TEM micrograph.

The device configuration and the corresponding energy level are shown in Figure 5a,b, respectively. The solution-processed MoO_x layer improved the hydrophilicity of graphene and thus assisted PEDOT:PSS to wet the surface more effectively. Moreover, the work function of graphene anode and highest occupied molecular orbital (HOMO) level of PEDOT:PSS are 5.1 and 5.0 eV, respectively, whereas the work function of MoO_x is 4.9 eV. Because of the slight energy level difference, the anode is favorable for hole extraction. The PEDOT:PSS layer played a double role of blocking the transport of electrons and facilitating the collection of holes. PbSe NC films were prepared via sequential spin-casting and ligand exchange using BDT. The BDT treatment increased film conductivity and enhanced light absorption. ZnO NCs were subsequently spin-casted onto the PbSe NC film and doped by ultraviolet (UV) exposure. Through UV photodoping, the conductivity of the ZnO NC film can be improved because of the passivation of electron traps on the ZnO surface.[27] The mobile electrons of ZnO can be trapped by gas molecules such as O_2, NO_2, and CO that are adsorbed on ZnO surface. By UV exposure, introduction of holes can result in desorption of molecular oxygen from the surface of the NC, allowing for a higher concentration of mobile electrons.[54,55] As a result, with direct UV excitation, the conduction band electron in ZnO has a long lifetime, most likely as a result of trapping of the corresponding hole.[50,56,57] The result is n-type doped ZnO NC film. A top aluminum cathode was deposited via thermal evaporation. Electrons drifted through the ZnO layer and were collected at the aluminum cathode, whereas holes drifted through the PEDOT:PSS layer and were collected at the graphene anode.

Current density–voltage ($J-V$) measurements were carried out under AM 1.5 G irradiation. The $J-V$ curves of the devices based on graphene and ITO anodes are shown in Figure 6. The $J-V$ characterization shows obvious diode behavior of the device fabricated on graphene under dark, indicating little leakage of current densities. Under illumination, the short-circuit current (J_{SC}), open-circuit voltage (V_{OC}), fill factor (FF), and power conversion efficiency (PCE) of the graphene/MoO_x-based device were 19.2 mA/cm^2, 0.42 V, 44.1%, and 3.56%, respectively. For the purpose of comparison, a control solar cell with an ITO anode was also fabricated and tested under identical experimental conditions, giving photovoltaic performance of V_{oc} = 0.41 V, J_{sc} = 20.37 mA/cm^2, FF = 48.9%, and PCE = 4.08%. The performance parameters of both devices are summarized in Table 1. We found that the graphene/

Table 1. Performance Details of Solar Cells Fabricated on Graphene/MoO_x and ITO Electrodes[a]

anode	J_{sc} (mA/cm^2)	V_{oc} (V)	FF (%)	PCE (%)
graphene/MoO_x	18.1 ± 1.1 (19.2)	0.41 ± 0.01 (0.42)	43.6 ± 0.5 (44.1)	3.31 ± 0.25 (3.56)
ITO	19.8 ± 0.9 (20.4)	0.40 ± 0.02 (0.41)	48.5 ± 0.4 (48.9)	3.79 ± 0.29 (4.08)

[a]Numbers in parentheses represent the values obtained for the best-performing cell. To account for experimental errors, eight devices of each type were measured to give the reported averages and deviations.

DOI: 10.1021/acsami.5b03894
ACS Appl. Mater. Interfaces 2015, 7, 21082–21088

MoO_x-based device has a V_{oc} similar to that of ITO-based device. This could be due to the fact that the V_{oc} in these heterostructure devices is mainly governed by the difference in the quasi-Fermi level of holes (E_{fp}) and electrons (E_{fn}). Meanwhile, the practical V_{oc} is also limited by the total recombination within the device. Therefore, efficient carrier transport is likely a path for enhancement of V_{oc}. The FF (44.1%) and J_{sc} (19.2 mA/cm^2) of graphene/MoO_x-based device were found to be lower than that of the ITO-based device, which is mainly caused by the higher sheet resistance of the graphene anode (several hundred Ω/sq) relative to that of the ITO film (10−20 Ω/sq). Figure 6c shows the EQE spectra of both devices. It is obvious that the ITO-based PbSe NC solar cell had a higher EQE than did the graphene-based device, mainly attributed to a lower sheet resistance of ITO, which is consistent with the conclusion obtained above. A lower sheet resistance of graphene film can be obtained via increasing the number of film layers; however, this operation results in a decrease in the transparency of the graphene film. Therefore, effective modification is needed to improve the conductivity and hydrophility property of graphene film while preserving the high transmittance. Additionally, interface modification of the graphene in terms of modifying its work function and surface free energy is also an important factor for charge or energy transfer. It is encouraging that the two cells exhibit similar device performances, indicating that monolayer graphene film is a promising candidate to replace ITO electrode.

4. CONCLUSIONS

We have shown a PbSe NC solar cell using solution-processed MoO_x-modified graphene film as the transparent electrode; the device efficiency of graphene-based devices reached 3.56%, which is very close to that of the ITO-based device (4.08%). This result demonstrates that the solution-processed MoO_x layer obtained from our approach is a promising and efficient interfacial material. Finally, CVD graphene with the characteristics of abundance, low cost, high conductivity, stability, transparency, and flexibility is promising to replace ITO in photovoltaic devices.

AUTHOR INFORMATION

Corresponding Authors

*E-mail: yuzhang@jlu.edu.cn.
*E-mail: wyu6000@gmail.com.

Author Contributions

H.W. and X.Z. contributed equally to this work.

Notes

The authors declare no competing financial interest.

ACKNOWLEDGMENTS

Y.W. was financially supported by the National 863 Program (2011AA050509) from ministry of science and technology of China; Y.Z. and W.G. received support from the National Natural Science Foundation of China (61106039, 51272084, 61306078, 61225018, and 61475062), the National Postdoctoral Foundation (2011049015), the Jilin Province Key Fund (20140204079GX), the Hong Kong Scholar Program (XJ2012022), and the State Key Laboratory on Integrated Optoelectronics (IOSKL2012ZZ12). H.W. was supported by the Taishan Scholarship and the Natural Science Foundation of Shandong Province (ZR2012FZ007); W.W.Y. was supported by NSF (1338346) and Louisiana Board of Regents.

REFERENCES

(1) Kumar, A.; Zhou, C. The Race to Replace Tin-Doped Indium Oxide: Which Material will win? *ACS Nano* **2010**, *4*, 11−14.
(2) He, S.; Li, S.; Wang, F.; Wang, A. Y.; Lin, J.; Tan, Z. a. Efficient Quantum Dot Light-Emitting Diodes with Solution-Processable Molybdenum Oxide as the Anode Buffer Layer. *Nanotechnology* **2013**, *24*, 175201.
(3) Andersson, A.; Johansson, N.; Bröms, P.; Yu, N.; Lupo, D.; Salaneck, W. R. Fluorine Tin Oxide as an Alternative to Indium Tin Oxide in Polymer LEDs. *Adv. Mater.* **1998**, *10*, 859−863.
(4) Novoselov, K. S.; Geim, A. K.; Morozov, S. V.; Jiang, D.; Zhang, Y.; Dubonos, S. V.; Grigorieva, I. V.; Firsov, A. A. Electric Field Effect in Atomically Thin Carbon Films. *Science* **2004**, *306*, 666−669.
(5) Li, X.; Cai, W.; An, J.; Kim, S.; Nah, J.; Yang, D.; Piner, R.; Velamakanni, A.; Jung, I.; Tutuc, E.; Banerjee, S. K.; Colombo, L.; Ruoff, R. S. Large-Area Synthesis of High-quality and Uniform Graphene Films on Copper Foils. *Science* **2009**, *324*, 1312−1314.
(6) Kim, K. S.; Zhao, Y.; Jang, H.; Lee, S. Y.; Kim, J. M.; Kim, K. S.; Ahn, J.-H.; Kim, P.; Choi, J.-Y.; Hong, B. H. Large-Scale Pattern Growth of Graphene Films for Stretchable Transparent Electrodes. *Nature* **2009**, *457*, 706−710.
(7) Bonaccorso, F.; Sun, Z.; Hasan, T.; Ferrari, A. C. Graphene Photonics and Optoelectronics. *Nat. Photonics* **2010**, *4*, 611−622.
(8) Wang, Z.; Puls, C. P.; Staley, N. E.; Zhang, Y.; Todd, A.; Xu, J.; Howsare, C. A.; Hollander, M. J.; Robinson, J. A.; Liu, Y. Technology Ready Use of Single Layer Graphene as a Transparent Electrode for Hybrid Photovoltaic Devices. *Phys. E* **2011**, *44*, 521−524.
(9) Zhang, D.; Choy, W. C. H.; Wang, C. C. D.; Li, X.; Fan, L.; Wang, K.; Zhu, H. Polymer Solar Cells with Gold Nanoclusters Decorated Multi-Layer Graphene as Transparent Electrode. *Appl. Phys. Lett.* **2011**, *99*, 223302.
(10) Seo, J.-T.; Han, J.; Lim, T.; Lee, K.-H.; Hwang, J.; Yang, H.; Ju, S. Fully Transparent Quantum Dot Light-Emitting Diode Integrated with Graphene Anode and Cathode. *ACS Nano* **2014**, *8*, 12476−12482.
(11) Shi, Y.; Kim, K. K.; Reina, A.; Hofmann, M.; Li, L.-J.; Kong, J. Work Function Engineering of Graphene Electrode via Chemical Doping. *ACS Nano* **2010**, *4*, 2689−2694.
(12) Jin, Z.; Yao, J.; Kittrell, C.; Tour, J. M. Large-Scale Growth and Characterizations of Nitrogen-Doped Monolayer Graphene Sheets. *ACS Nano* **2011**, *5*, 4112−4117.
(13) Yan, L.; Zhang, Y.; Zhang, X.; Zhao, J.; Wang, Y.; Zhang, T.; Jiang, Y.; Gao, W.; Yin, J.; Zhao, J.; Yu, W. W. Single Layer Graphene Electrodes for Quantum Dot Light Emitting Diodes. *Nanotechnology* **2015**, *26*, 135201.
(14) Wang, Y.; Chen, X.; Zhong, Y.; Zhu, F.; Loh, K. P. Large Area, Continuous, Few-Layered Graphene as Anodes in Organic Photovoltaic Devices. *Appl. Phys. Lett.* **2009**, *95*, 063302.
(15) Zhang, D.; Xie, F.; Lin, P.; Choy, W. C. H. Al-TiO_2 Composite-Modified Single-Layer Graphene as an Efficient Transparent Cathode for Organic Solar Cells. *ACS Nano* **2013**, *7*, 1740−1747.
(16) Wang, Y.; Tong, S. W.; Xu, X. F.; Özyilmaz, B.; Loh, K. P. Interface Engineering of Layer-by-Layer Stacked Graphene Anodes for High-Performance Organic Solar Cells. *Adv. Mater.* **2011**, *23*, 1514−1518.
(17) Park, H.; Brown, P. R.; Bulović, V.; Kong, J. Graphene As Transparent Conducting Electrodes in Organic Photovoltaics: Studies in Graphene Morphology, Hole Transporting Layers, and Counter Electrodes. *Nano Lett.* **2012**, *12*, 133−140.
(18) Zhang, J.; Gao, J.; Church, C. P.; Miller, E. M.; Luther, J. M.; Klimov, V. I.; Beard, M. C. PbSe Quantum Dot Solar Cells with More than 6% Efficiency Fabricated in Ambient Atmosphere. *Nano Lett.* **2014**, *14*, 6010−6015.
(19) Semonin, O. E.; Luther, J. M.; Choi, S.; Chen, H.-Y.; Gao, J.; Nozik, A. J.; Beard, M. C. Peak External Photocurrent Quantum Efficiency Exceeding 100% via MEG in a Quantum Dot Solar Cell. *Science* **2011**, *334*, 1530−1533.
(20) Pattantyus-Abraham, A. G.; Kramer, I. J.; Barkhouse, A. R.; Wang, X.; Konstantatos, G.; Debnath, R.; Levina, L.; Raabe, I.;

DOI: 10.1021/acsami.5b03894
ACS Appl. Mater. Interfaces 2015, 7, 21082−21088

Nazeeruddin, M. K.; Grätzel, M.; Sargent, E. H. Depleted-Heterojunction Colloidal Quantum Dot Solar Cells. *ACS Nano* **2010**, *4*, 3374−3380.
(21) Ma, W.; Swisher, S. L.; Ewers, T.; Engel, J.; Ferry, V. E.; Atwater, H. A.; Alivisatos, A. P. Photovoltaic Performance of Ultrasmall PbSe Quantum Dots. *ACS Nano* **2011**, *5*, 8140−8147.
(22) Ma, W.; Luther, J. M.; Zheng, H.; Wu, Y.; Alivisatos, A. P. Photovoltaic Devices Employing Ternary PbS_xSe_{1-x} Nanocrystals. *Nano Lett.* **2009**, *9*, 1699−1703.
(23) Jean, J.; Chang, S.; Brown, P. R.; Cheng, J. J.; Rekemeyer, P. H.; Bawendi, M. G.; Gradečak, S.; Bulović, V. ZnO Nanowire Arrays for Enhanced Photocurrent in PbS Quantum Dot Solar Cells. *Adv. Mater.* **2013**, *25*, 2790−2796.
(24) Hoye, R. L. Z.; Ehrler, B.; Böhm, M. L.; Muñoz-Rojas, D.; Altamimi, R. M.; Alyamani, A. Y.; Vaynzof, Y.; Sadhanala, A.; Ercolano, G.; Greenham, N. C.; Friend, R. H.; MacManus-Driscoll, J. L.; Musselman, K. P. Improved Open- Circuit Voltage in ZnO−PbSe Quantum Dot Solar Cells by Understanding and Reducing Losses Arising from the ZnO Conduction Band Tail. *Adv. Energy Mater.* **2014**, *4*, 1301544.
(25) Ehrler, B.; Walker, B. J.; Böhm, M. L.; Wilson, M. W. B.; Vaynzof, Y.; Friend, R. H.; Greenham, N. C. In Situ Measurement of Exciton Energy in Hybrid Singlet-Fission Solar Cells. *Nat. Commun.* **2012**, *3*, 1019.
(26) Ehrler, B.; Musselman, K. P.; Böhm, M. L.; Morgenstern, F. S. F.; Vaynzof, Y.; Walker, B. J.; MacManus-Driscoll, J. L.; Greenham, N. C. Preventing Interfacial Recombination in Colloidal Quantum Dot Solar Cells by Doping the Metal Oxide. *ACS Nano* **2013**, *7*, 4210−4220.
(27) Choi, J. J.; Lim, Y.-F.; Santiago-Berrios, M. E. B.; Oh, M.; Hyun, B.-R.; Sun, L.; Bartnik, A. C.; Goedhart, A.; Malliaras, G. G.; Abruña, H. D.; Wise, F. W.; Hanrath, T. PbSe Nanocrystal Excitonic Solar Cells. *Nano Lett.* **2009**, *9*, 3749−3755.
(28) Kuo, C.-Y.; Su, M.-S.; Ku, C.-S.; Wang, S.-M.; Lee, H.-Y.; Wei, K.-H. Ligands affect the Crystal Structure and Photovoltaic Performance of Thin Films of PbSe Quantum Dots. *J. Mater. Chem.* **2011**, *21*, 11605−11612.
(29) McDonald, S. A.; Konstantatos, G.; Zhang, S.; Cyr, P. W.; Klem, E. J. D.; Levina, L.; Sargent, E. H. Solution-Processed PbS Quantum Dot Infrared Photodetectors and Photovoltaics. *Nat. Mater.* **2005**, *4*, 138−142.
(30) Ning, Z.; Zhitomirsky, D.; Adinolfi, V.; Sutherland, B.; Xu, J.; Voznyy, O.; Maraghechi, P.; Lan, X.; Hoogland, S.; Ren, Y.; Sargent, E. H. Graded Doping for Enhanced Colloidal Quantum Dot Photovoltaics. *Adv. Mater.* **2013**, *25*, 1719−1723.
(31) Tang, J.; Liu, H.; Zhitomirsky, D.; Hoogland, S.; Wang, X.; Furukawa, M.; Levina, L.; Sargent, E. H. Quantum Junction Solar Cells. *Nano Lett.* **2012**, *12*, 4889−4894.
(32) Ning, Z.; Dong, H.; Zhang, Q.; Voznyy, O.; Sargent, E. H. Solar Cells Based on Inks of n-Type Colloidal Quantum Dots. *ACS Nano* **2014**, *8*, 10321−10327.
(33) Ning, Z.; Voznyy, O.; Pan, J.; Hoogland, S.; Adinolfi, V.; Xu, J.; Li, M.; Kirmani, A. R.; Sun, J.-P.; Minor, J.; Kemp, K. W.; Dong, H.; Rollny, L.; Labelle, A.; Carey, G.; Sutherland, B.; Hill, I.; Amassian, A.; Liu, H.; Tang, J.; Bakr, O. M.; Sargent, E. H. Air-Stable n-Type Colloidal Quantum Dot Solids. *Nat. Mater.* **2014**, *13*, 822−828.
(34) Chuang, C.-H. M.; Brown, P. R.; Bulović, V.; Bawendi, M. G. Improved Performance and Stability in Quantum Dot Solar Cells through Band Alignment Engineering. *Nat. Mater.* **2014**, *13*, 796−801.
(35) Kirmani, A. R.; Carey, G. H.; Abdelsamie, M.; Yan, B.; Cha, D.; Rollny, L. R.; Cui, X.; Sargent, E. H.; Amassian, A. Effect of Solvent Environment on Colloidal-Quantum-Dot Solar-Cell Manufacturability and Performance. *Adv. Mater.* **2014**, *26*, 4717−4723.
(36) Park, H.; Chang, S.; Jean, J.; Cheng, J. J.; Araujo, P. T.; Wang, M.; Bawendi, M. G.; Dresselhaus, M. S.; Bulović, V.; Kong, J.; Gradečak, S. Graphene Cathode-Based ZnO Nanowire Hybrid Solar Cells. *Nano Lett.* **2013**, *13*, 233−239.
(37) Lin, C.-C.; Wang, D.-Y.; Tu, K.-H.; Jiang, Y.-T.; Hsieh, M.-H.; Chen, C.-C.; Chen, C.-W. Enhanced Infrared Light Harvesting of Inorganic Nanocrystal Photovoltaic and Photodetector on Graphene Electrode. *Appl. Phys. Lett.* **2011**, *98*, 263509.
(38) Park, H.; Chang, S.; Zhou, X.; Kong, J.; Palacios, T.; Gradečak, S. Flexible Graphene Electrode-Based Organic Photovoltaics with Record-High Efficiency. *Nano Lett.* **2014**, *14*, 5148−5154.
(39) Lee, Y.-Y.; Tu, K.-H.; Yu, C.-C.; Li, S.-S.; Hwang, J.-Y.; Lin, C.-C.; Chen, K.-H.; Chen, L.-C.; Chen, H.-L.; Chen, C.-W. Top Laminated Graphene Electrode in a Semitransparent Polymer Solar Cell by Simultaneous Thermal Annealing/Releasing Method. *ACS Nano* **2011**, *5*, 6564−6570.
(40) Gomez De Arco, L.; Zhang, Y.; Schlenker, C. W.; Ryu, K.; Thompson, M. E.; Zhou, C. Continuous, Highly Flexible, and Transparent Graphene Films by Chemical Vapor Deposition for Organic Photovoltaics. *ACS Nano* **2010**, *4*, 2865−2873.
(41) Park, H.; Howden, R. M.; Barr, M. C.; Bulović, V.; Gleason, K.; Kong, J. Organic Solar Cells with Graphene Electrodes and Vapor Printed Poly(3,4-ethylenedioxythiophene) as the Hole Transporting Layers. *ACS Nano* **2012**, *6*, 6370−6377.
(42) Hsu, C.-L.; Lin, C.-T.; Huang, J.-H.; Chu, C.-W.; Wei, K.-H.; Li, L.-J. Layer-by-Layer Graphene/TCNQ Stacked Films as Conducting Anodes for Organic Solar Cells. *ACS Nano* **2012**, *6*, 5031−5039.
(43) Li, N.; Oida, S.; Tulevski, G. S.; Han, S.-J.; Hannon, J. B.; Sadana, D. K.; Chen, T.-C. Efficient and Bright Organic Light-Emitting Diodes on Single-Layer Graphene Electrodes. *Nat. Commun.* **2013**, *4*, 2294.
(44) Yu, W. W.; Falkner, J. C.; Shih, B. S.; Colvin, V. L. Preparation and Characterization of Monodisperse PbSe Semiconductor Nanocrystals in a Noncoordinating Solvent. *Chem. Mater.* **2004**, *16*, 3318−3322.
(45) Yan, L.; Zhang, Y.; Zhang, T.; Feng, Y.; Zhu, K.; Wang, D.; Cui, T.; Yin, J.; Wang, Y.; Zhao, J.; Yu, W. W. Tunable near-Infrared Luminescence of PbSe Quantum Dots for Multigas Analysis. *Anal. Chem.* **2014**, *86*, 11312−11318.
(46) Wu, H.; Zhang, Y.; Yan, L.; Jiang, Y.; Zhang, T.; Feng, Y.; Chu, H.; Wang, Y.; Zhao, J.; Yu, W. W. Temperature Effect on Colloidal PbSe Quantum Dot-Filled Liquid-Core Optical Fiber. *Opt. Mater. Express* **2014**, *4*, 1856−1865.
(47) Zhang, Y.; Dai, Q.; Li, X.; Zou, B.; Wang, Y.; Yu, W. W. Beneficial Effect of Tributylphosphine to the Photoluminescence of PbSe and PbSe/CdSe Nanocrystals. *J. Nanopart. Res.* **2011**, *13*, 3721−3729.
(48) Zhang, Y.; Dai, Q.; Li, X.; Liang, J.; Colvin, V. L.; Wang, Y.; Yu, W. W. PbSe/CdSe and PbSe/CdSe/ZnSe Hierarchical Nanocrystals and Their Photoluminescence. *Langmuir* **2011**, *27*, 9583−9587.
(49) Zhang, Y.; Dai, Q.; Li, X.; Cui, Q.; Gu, Z.; Zou, B.; Wang, Y.; Yu, W. W. Formation of PbSe/CdSe Core/Shell Nanocrystals for Stable Near-Infrared High Photoluminescence Emission. *Nanoscale Res. Lett.* **2010**, *5*, 1279−1283.
(50) Beek, W. J. E.; Wienk, M. M.; Kemerink, M.; Yang, X.; Janssen, R. A. J. Hybrid Zinc Oxide Conjugated Polymer Bulk Heterojunction Solar Cells. *J. Phys. Chem. B* **2005**, *109*, 9505−9516.
(51) Jasieniak, J. J.; Seifter, J.; Jo, J.; Mates, T.; Heeger, A. J. A Solution-Processed MoO_x Anode Interlayer for Use within Organic Photovoltaic Devices. *Adv. Funct. Mater.* **2012**, *22*, 2594−2605.
(52) Tan, Z. a.; Qian, D.; Zhang, W.; Li, L.; Ding, Y.; Xu, Q.; Wang, F.; Li, Y. Efficient and Stable Polymer Solar Cells with Solution-Processed Molybdenum Oxide Interfacial Layer. *J. Mater. Chem. A* **2013**, *1*, 657−664.
(53) Li, X.; Zhu, Y.; Cai, W.; Borysiak, M.; Han, B.; Chen, D.; Piner, R. D.; Colombo, L.; Ruoff, R. S. Transfer of Large-Area Graphene Films for High-Performance Transparent Conductive Electrodes. *Nano Lett.* **2009**, *9*, 4359−4363.
(54) Lakhwani, G.; Roijmans, R. F. H.; Kronemeijer, A. J.; Gilot, J.; Janssen, R. A. J.; Meskers, S. C. J. Probing Charge Carrier Density in a Layer of Photodoped ZnO Nanoparticles by Spectroscopic Ellipsometry. *J. Phys. Chem. C* **2010**, *114*, 14804−14810.
(55) Morfa, A. J.; MacDonald, B. I.; Subbiah, J.; Jasieniak, J. J. Understanding the Chemical Origin of Improved Thin-Film Device

DOI: 10.1021/acsami.5b03894
ACS Appl. Mater. Interfaces 2015, 7, 21082−21088

Performance from Photodoped ZnO Nanoparticles. *Sol. Energy Mater. Sol. Cells* **2014**, *124*, 211−216.
(56) van Dijken, A.; Meulenkamp, E. A.; Vanmaekelbergh, D.; Meijerink, A. The Luminescence of Nanocrystalline ZnO Particles: the Mechanism of the Ultraviolet and Visible Emission. *J. Lumin.* **2000**, *87*−*89*, 454−456.
(57) van Dijken, A.; Meulenkamp, E. A.; Vanmaekelbergh, D.; Meijerink, A. Identification of the Transition Responsible for the Visible Emission in ZnO using Quantum Size Effects. *J. Lumin.* **2000**, *90*, 123−128.
(58) Zhang, X.; Zhang, Y.; Yan, L.; Ji, C.; Wu, H.; Wang, Y.; Wang, P.; Zhang, T.; Wang, Y.; Cui, T.; Zhao, J.; Yu, W. W. High Photocurrent PbSe Solar Cells with Thin Active Layers. *J. Mater. Chem. A* **2015**, *3*, 8501−8507.
(59) Ko, D.-K.; Brown, P. R.; Bawendi, M. G.; Bulović, V. p-i-n Heterojunction Solar Cells with a Colloidal Quantum-Dot Absorber Layer. *Adv. Mater.* **2014**, *26*, 4845−4850.

DOI: 10.1021/acsami.5b03894
ACS Appl. Mater. Interfaces 2015, 7, 21082−21088